Topology Optimization Design and Experiment of a Soft Pneumatic Bending Actuator for Grasping Applications

Chih-Hsing Liu ⬤, Li-Jyun Chen, Jui-Chih Chi, and Jyun-Yi Wu

Abstract—Soft pneumatic bending actuators are commonly used in robotic grasping applications and can be applied for handling both delicate and irregularly shaped objects. Because these soft pneumatic actuators are typically embedded with multiple air chambers inside soft, thin structures, their maximum payloads are usually low compared to rigid designs of similar size. This article presents a soft pneumatic bending actuator design using a topology optimization procedure that can maximize the bending capability and thus increase the allowable payload of soft grippers that consist of multiple pneumatic bending actuators. After an optimum design is obtained, multiple identical actuators are prototyped through a molding process using a silicone rubber material. Both two-fingered and three-fingered soft grippers are developed using the topology-optimized pneumatic bending actuators. Experiments, including a bending angle test, an output force test, and a payload test, are conducted in this study, and the results are compared against the test results of the commercial SRT soft pneumatic actuator. The experimental results show that the bending angle for the developed bending actuator is 111 degrees on average of 10 tests at an input pressure of 50 kPa. The output force is 9.45 N at an input pressure of 80 kPa, while the maximum payloads of the two-fingered and three-fingered grippers are 2.66 kg and 5.12 kg, respectively.

Index Terms—Soft bending actuator, soft pneumatic actuator, soft finger, soft gripper, topology optimization, soft robot.

I. INTRODUCTION

THE DEVELOPMENT of a robotic gripper for handling of a wide range of objects with various sizes, shapes, and degrees of hardness has drawn considerable attention over the years [1]–[8]. The end-effector is typically the only interface between a robot and its working environment. Therefore, the overall performance of a robot highly depends on its end-effector [9]. Data-driven grasp synthesis approaches for finding a grasp configuration that satisfies a set of criteria relevant for a grasping task can be classified into three categories: known, familiar, and

unknown objects, based on what is known *a priori* about the target [10]. Traditional robot manipulators have rigid underlying structures that often encounter difficulties during operating in unstructured and highly congested environments [11]. On the other hand, soft, deformable robots have many advantages over rigid robots, including providing safer, more robust interactions and adaptive behaviors that use mechanical intelligence suitable for dealing with unknown objects in a complex environment [12]. Several control strategies, such as the use of a feedforward controller based on both rigid-body and flexible modes [13], and a constrained linear quadratic optimization algorithm [14] can be used in vibration suppression of flexible systems.

Soft grippers have the potential to interact with humans and complex environments in more sophisticated ways than rigid robots [15] and have been used in many different fields, including food packaging [16], [17], poultry processing [18]–[20], force regulation [21]–[23], and underwater applications [24], [25]. Typically, soft grippers are actuated either pneumatically [2], [3], [6], [16], [17], [24], [26] or electrically [4], [5], [7], [23], [25], [27]–[30]. Most pneumatic soft grippers have three or four identical pneumatic actuators (or fingers) with multiple air chambers inside the actuator structures. These pneumatic actuators are usually made of soft materials such as silicone rubber or other elastomers [31]. When a soft actuator is pressurized by the supply air, the embedded air chambers inflate, which leads to the bending of the actuator.

One common issue for pneumatic soft grippers is that the maximum load capacity is usually low comparing to rigid grippers or other motor-driven compliant gripper designs [5], [7], [27], [29] of similar size. For example, the maximum payload of the four-fingered soft pneumatic gripper presented by Wang *et al.* [16] is 75.2 g at an input pressure of 60 kPa. Zhang *et al.* [6] developed a pneumatic bending actuator for gripper application using a topology optimization method. The experimental results showed that each gripper finger was able to undergo a 14.7 degree free travel bending and could exert a 0.23 N grasping force at a 60 kPa actuation pressure. Another design presented by Zhang *et al.* [26] showed that their multi-material three-fingered pneumatic soft gripper can exert a higher payload and grip objects with weights as high as 167.9 g. In order to increase the payload, a dual-mode four-fingered pneumatic soft gripper was proposed [17] for grasping and suction of food products. According to the test results, the dual-mode gripper can lift a 274g object in the grasping mode at a pressure of 70 kPa and a 1.07 kg object in the suction mode at a pressure of approximately −90 kPa. An octopus arm-inspired tapered soft actuator with multiple suckers was also presented [32]. It enables the actuator

to improve its grasping capabilities through both bending and sunction functions. In order to develop a high-force pnematic gripper, Yap *et al.* [3] uses a harder thermoplastic elastomer to prototype a pneumatic actuator that can allow to be pressurized up to approximately 400 kPa.

Motivated by the need to increase the maximum load capacity of the soft grippers that consist of multiple soft pneumatic bending actuators, this study is aimed toward designing a soft pneumatic bending actuator using a topology optimization procedure that can maximize its bending capabilities at a low supply pressure ($<$100 kPa) and thus increase the allowable payload of a multi-fingered pneumatic gripper. Topology optimization is a numerical method that can optimize the material layout within a given design domain. It has been used to synthesize various designs, such as soft fingers and grippers [5]–[7], [26]–[29], constant-force mechanisms [22], [23], [33], and compliant inverters [34]–[36]. The mutual potential energy (MPE), which is the mutual energy due to two different sets of loading at input and output points, is used as the objective function in this article to design the pneumatic bending actuator instead of using a displacement at a specified point [6], [26], [28] or a composite strain energy formulation [5], [7], [27], [29]. In addition, a three-dimensional (3D) domain is used in this study.

In the present work, after an optimum design is obtained through the presented topology optimization method, multiple identical actuators are prototyped through the molding process using the Dragon Skin 30 silicone rubber material. Both two-fingered and three-fingered soft grippers are developed using topology-optimized pneumatic bending actuators. A bending angle test, an output force test, and a payload test are performed in this study, and the experimental results are compared against the test results for a commercial SRT soft pneumatic actuator [37]. The experimental results showed that the soft pneumatic bending actuator developed in this work is superior to the commercial SRT actuator in terms of maximizing the bending angle and the output force since an optimal material layout of the interface structure is identified that leads to a larger amount of bending deflection and thus increase the payloads of multi-fingered grippers.

II. TOPOLOGY OPTIMIZATION METHOD

The topology optimization problem begins from the definition of the design domain, the boundary conditions, and the parameters. A density filter [38] is used to prevent the appearance of checkerboard patterns as well as mesh dependency problems. The filtered element density ($\tilde{x}_i$) of the ith element can be calculated by

$$\tilde{x}_i = \frac{\sum_{j \in N_{e,i}} w_{ij} v_j x_j}{\sum_{j \in N_{e,i}} w_{ij} v_j}, w_{ij} = \max\left(0, r_{\min} - r_{ij}\right) \quad (1)$$

where $N_{e,\,i}$ is the set of elements within the filtering radius ($r_{\min}$) around the i_{th} element; w_{ij} is the weight function; v_j is the volume of the element; x_j is the element density that serves as the design variable with values ranging from 0 to 1, and r_{ij} is the distance between the ith element and the jth element.

The objective function of the topology optimization problem in this study is intended to maximize the mutual potential energy of the synthesized design, which can be formulated as

$$MPE = \mathbf{U}_2^T \mathbf{K} \mathbf{U}_1 \quad (2)$$

where *MPE* is the mutual potential energy; $\mathbf{K}$ is the global stiffness matrix; $\mathbf{U}_1$ is the global displacement vector corresponding to the global input force vector $\mathbf{F}_1$, and $\mathbf{U}_2$ is the global displacement vector corresponding to the dummy output force vector $\mathbf{F}_2$. Maximizing the MPE allows a design to maximize its nodal displacements at output points while the input forces are applied at input points.

In addition, the displacement of each node is calculated according to Hooke's law.

$$\mathbf{K}\mathbf{U}_1 = \mathbf{F}_1, \mathbf{K}\mathbf{U}_2 = \mathbf{F}_2 \quad (3)$$

The sensitivity for the objective function in (2) with respect to the filtered element density can be calculated by

$$\frac{\partial MPE}{\partial \tilde{x}} = \frac{\partial}{\partial \tilde{x}} \left(\mathbf{U}_2^T \mathbf{K} \mathbf{U}_1\right)$$

$$= \frac{\partial \mathbf{U}_2^T}{\partial \tilde{x}} \mathbf{K} \mathbf{U}_1 + \mathbf{U}_2^T \frac{\partial \mathbf{K}}{\partial \tilde{x}} \mathbf{U}_1 + \mathbf{U}_2^T \mathbf{K} \frac{\partial \mathbf{U}_1}{\partial \tilde{x}}$$

$$= \mathbf{U}_1^T \mathbf{K} \frac{\partial \mathbf{U}_2}{\partial \tilde{x}} + \mathbf{U}_2^T \frac{\partial \mathbf{K}}{\partial \tilde{x}} \mathbf{U}_1 + \mathbf{U}_2^T \mathbf{K} \frac{\partial \mathbf{U}_1}{\partial \tilde{x}} \quad (4)$$

The derivatives of the two equations in (3) with respect to the filtered element density yield

$$\begin{cases} \frac{\partial \mathbf{K}}{\partial \tilde{x}} \mathbf{U}_1 + \mathbf{K} \frac{\partial \mathbf{U}_1}{\partial \tilde{x}} = 0, \mathbf{K} \frac{\partial \mathbf{U}_1}{\partial \tilde{x}} = -\frac{\partial \mathbf{K}}{\partial \tilde{x}} \mathbf{U}_1 \\ \frac{\partial \mathbf{K}}{\partial \tilde{x}} \mathbf{U}_2 + \mathbf{K} \frac{\partial \mathbf{U}_2}{\partial \tilde{x}} = 0, \mathbf{K} \frac{\partial \mathbf{U}_2}{\partial \tilde{x}} = -\frac{\partial \mathbf{K}}{\partial \tilde{x}} \mathbf{U}_2 \end{cases} \quad (5)$$

Substituting (5) into (4) yields

$$\frac{\partial MPE}{\partial \tilde{x}} = -\mathbf{U}_1^T \frac{\partial \mathbf{K}}{\partial \tilde{x}} \mathbf{U}_2 \quad (6)$$

For a single element

$$\frac{\partial MPE}{\partial \tilde{x}_i} = -\mathbf{u}_{1i}^T \frac{\partial \mathbf{k}_i}{\partial \tilde{x}_i} \mathbf{u}_{2i} \quad (7)$$

where $\mathbf{u}_{1i}$ is the displacement vector of the i_{th} element corresponding to the input force vector; $\mathbf{u}_{2i}$ is the displacement vector of the i_{th} element corresponding to the output force vector, and $\mathbf{k}_i$ is the stiffness matrix of the i_{th} element, which is linearly proportional to the elastic modulus of the i_{th} element according to the following relationship based on the concept of a solid isotropic material with penalization (SIMP) [38].

$$\mathbf{k}_i = E_i \mathbf{k}_0 = \left(E_{\min} + \tilde{\boldsymbol{x}}_i^p \left(E_0 - E_{\min}\right)\right) \mathbf{k}_0 \quad (8)$$

where E_i is the elastic modulus of the ith element; $\mathbf{k}_0$ is the stiffness matrix of the ith element with a unit elastic modulus; $E_{\min}$ is the minimum elastic modulus with a small positive value close to zero; p is the penalty parameter, and E_0 is the elastic modulus of the original material. According to (8), if a filtered element density is equal to 1, it is a solid element ($E_{\mathrm{i}} = E_0$); if a filtered element density is equal to 0, it is a void element ($E_{\mathrm{i}} = E_{\min}$); if a filtered element density is between 0 and 1, it is a grey element.

Substituting (8) into (7) yields the sensitivity for the MPE with respect to the filtered element density.

$$\frac{\partial MPE}{\partial \tilde{x}_i} = -p \left(E_0 - E_{\min}\right) \tilde{x}_i^{p-1} \mathbf{u}_{1i}^T \mathbf{k}_0 \mathbf{u}_{2i} \quad (9)$$

Based on (1) and (9), the sensitivity, α_i, for the MPE with respect to the element density can be obtained according to the
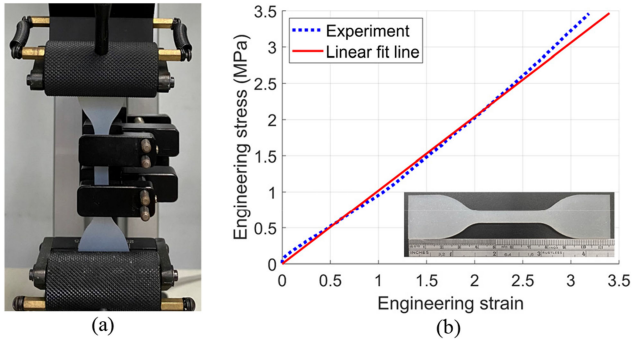
Fig. 1. Tensile test for the Dragon Skin 30 silicone rubber. (a) Experimental setup. (b) Engineering stress versus engineering strain curve. The linear fit line is with an elastic modulus of 1.02 MPa.

chain rule.

$$\alpha_i = \frac{\partial MPE}{\partial x_i} = \frac{\partial MPE}{\partial \tilde{x}_i} \frac{\partial \tilde{x}_i}{\partial x_i} \tag{10}$$

The objective function value and the sensitivity for each element can be calculated respectively based on (2) and (10). The design variables are updated using the method of moving asymptotes (MMA) [39], which converts the MPE maximization problem into a negative MPE minimization problem in practice. The optimization procedure is converged if the following two convergence conditions are satisfied. The first condition is that the relative difference ratio for the objective function value for each successive iterations is smaller than an allowable objective function tolerance. The second condition is that the difference between the calculated volume and the target volume after topology optimization is smaller than an allowable volume tolerance.

III. TOPOLOGY OPTIMIZATION DESIGN FOR THE SOFT PNEUMATIC BENDING ACTUATOR

The discussed optimization method is used to design the soft pneumatic bending actuator. In order to identify the value of elastic modulus for the Dragon Skin 30 silicone rubber, a tensile test as shown in Fig. 1 is performed, where Fig. 1(a) shows the experimental setup, and Fig. 1(b) provides the experimental stress-strain curve and a linear fit line with an elastic modulus of 1.02 MPa. The results show that the material model for Dragon Skin 30 silicone rubber can be approximated using a linear elastic model in numerical computation when an engineering strain is within 3.

One segment of the soft pneumatic bending actuator shown in Fig. 2 is used as the analysis domain for the three-dimensional topology optimization. The analyzed segment has three air chambers, as shown in Fig. 2, for which the size of each chamber is $2\,\mathrm{mm} \times 20\,\mathrm{mm} \times 46\,\mathrm{mm}$. The analysis domain consists of one design domain, three solid non-design domains (elements have an element density of 1), and three void non-design domains (elements have an element density of 0). The element densities in the design domain can be updated iteratively in a range from 0 to 1. The three air chambers are defined as the void non-design domains, while the surrounding regions around the three air chambers with a thickness of 2 mm are defined as the solid non-design domain.

The input forces are applied normally at the nodes on the inner surfaces of the air chambers. The sum of the forces is equal to
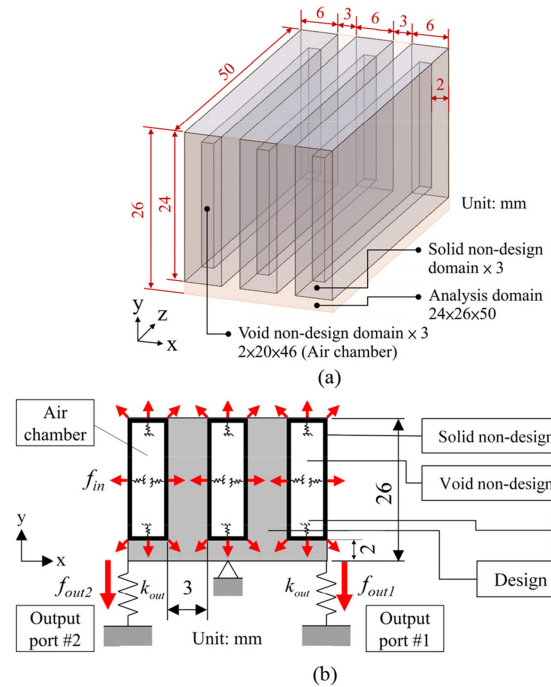

Fig. 2. Analysis domain for one segment of the soft pneumatic bending actuator. (a) 3D view. (b) 2D view.

TABLE I
PARAMETERS FOR TOPOLOGY OPTIMIZATION

Parameter	Value
Elastic modulus (E_0)	1.02MPa
Minimum elastic modulus ($E_{\min}$)	10^{-9}MPa
Poisson's ratio	0.49
Analysis domain	24mm×26mm×50mm
Element size	1mm×1mm×1mm
Filtering radius ($r_{\min}$)	3mm
Penalty parameter (p)	3
Volume fraction	0.645
Number of nodes for applying the input forces	2106
Number of nodes at the output port#1	51
Number of nodes at the output port#2	51
Input spring stiffness	1/2106 N/mm
Output spring stiffness	1/102 N/mm

1. The geometrically nonlinear finite element formulation is not considered due to the nodal displacements are small in topology optimization process while the usage of the small dummy forces, and the existence of the numerical springs at the force applied nodes as illustrated in Fig. 2(b). The fixed region is the middle portion of the bottom surface, whereas the target output ports are at the two ends, as denoted in Fig. 2(b). Maximizing the MPE of the analysis domain allows a design to maximize its nodal displacements at the target output ports (two ends) while the input forces are applied, which is equivalent to maximizing the bending capability of the actuator. The analysis domain is discretized with linear hexahedral 1 mm × 1 mm × 1 mm elements. The topology optimization procedure discussed in Section II is used to identify the optimal material layout of the design domain, as shown in Fig. 2(b). The numerical parameters used in the topology optimization are summarized in Table I.
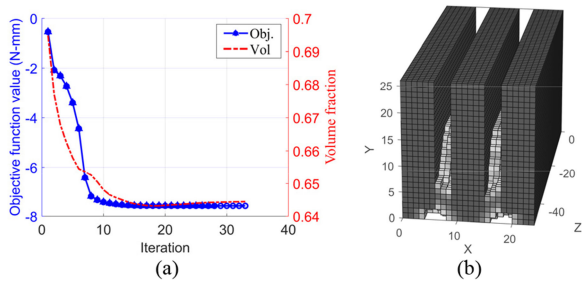
Fig. 3. Topology optimization results. (a) Iterative results for the objective function value and the volume fraction. (b) Topology optimization result for one segment of the soft pneumatic bending actuator.
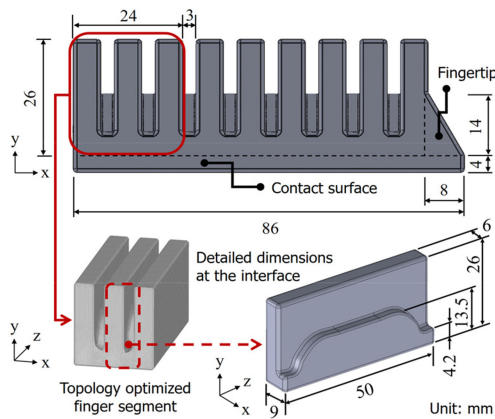

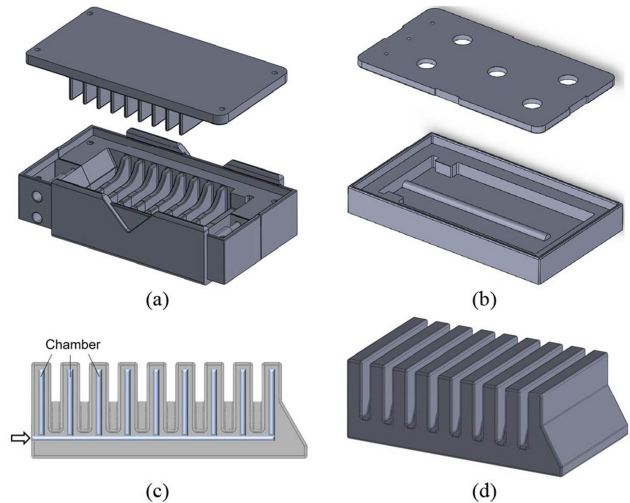Fig. 4. Design model of the soft pneumatic bending actuator.

Fig. 5. Mold design for the soft pneumatic bending actuator. (a) Mold design for the upper portion of the actuator. (b) Mold design for the lower portion of the actuator. (c) Air intake design. (d) Soft pneumatic bending actuator.
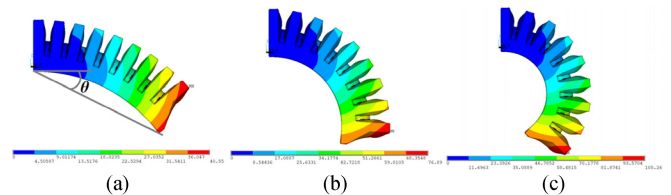

Fig. 6. Results of the geometrically nonlinear finite element analysis for the bending deformation of the developed soft actuator under different air pressures. (a) 10 kPa. (b) 20 kPa. (c) 30 kPa.

The topology optimization process converged after 33 iterations. Fig. 3(a) shows the iterative results for the objective function value and the volume fraction. Fig. 3(b) shows the topology optimization result for one segment (with three air chambers) of the soft pneumatic bending actuator. The design model for the soft pneumatic bending actuator is shown in Fig. 4 based on the optimized finger segment obtained from the topology optimization. The detailed dimensions at the interface between the chamber structures are shown in Fig. 4. As shown in Fig. 4, the final design of the soft pneumatic bending actuator consists of three optimized finger segments in series (with 9 air chambers in total), a fingertip structure, and a contact surface structure. The length, height, and width of the soft pneumatic bending actuator are 86 mm, 30 mm, and 50 mm, respectively. The soft pneumatic bending actuator is prototyped through a molding process using the Dragon Skin 30 silicone rubber material. The mold design for the upper portion of the actuator is shown in Fig. 5(a), whereas Fig. 5(b) shows the mold design for the lower portion of the actuator. Fig. 5(c) shows the air intake and connecting channel design at a cross section of the mid-surface in the width direction of the actuator. Fig. 5(d) shows a 3D view of the soft pneumatic bending actuator.

IV. FINITE ELEMENT ANALYSIS

To investigate the performance of the design obtained in Fig. 5(d), a three-dimensional finite element model was developed using Ansys commercial finite element analysis (FEA) software to evaluate the design. The results of the geometrically nonlinear FEA for the bending deformation of the developed actuator under different air pressures (10, 20, and 30 kPa) are provided in Fig. 6, where the angle θ as denoted in Fig. 6(a) is the bending angle used to quantify the amount of bending taking place in the soft actuator. The bending angles for the three air pressure conditions in Fig. 6 are estimated to be 26°, 51°, and 74°, respectively. The deformation plots in Fig. 6 are displacement contours in mm units. The results demonstrate that the developed pneumatic actuator can provide adequate bending deformation at low supply pressures. The maximum equivalent strain values for the bending actuator at the input pressure of 10, 20, and 30 kPa are 0.188, 0.357, and 0.511, respectively, which are within the nearly linear range according to the stress-strain curve provided in Fig. 1(b) thus the linear elastic material model is used in this study.

To investigate the effectiveness of the topology-optimized design shown in Fig. 7(a), three additional actuator designs with different interface structures, as shown in Fig. 7(b)–(d), are analyzed in order to compare their maximum bending angles under different input pressures. As shown in Fig. 7, Design 2 is a design with more material at the interface structure comparing to the topology-optimized design (Design 1), whereas Design 3 is a design with less interface material. Design 4 is a design with an interface structure similar to the commercial SRT soft pneumatic bending actuator [37].

The results of the analysis for the three additional designs are provided in Fig. 8, where Fig. 8(a)–(c) show the deformed
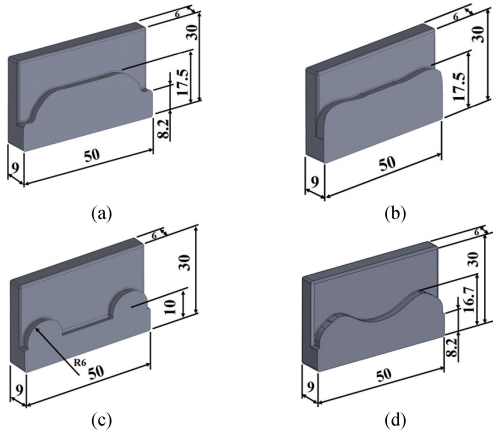
Fig. 7. Analysis examples with different interface structures. (a) Design 1: topology-optimized design. (b) Design 2. (c) Design 3. (d) Design 4.

Fig. 9. Bending deformation of the developed soft pneumatic actuator at different air pressures.
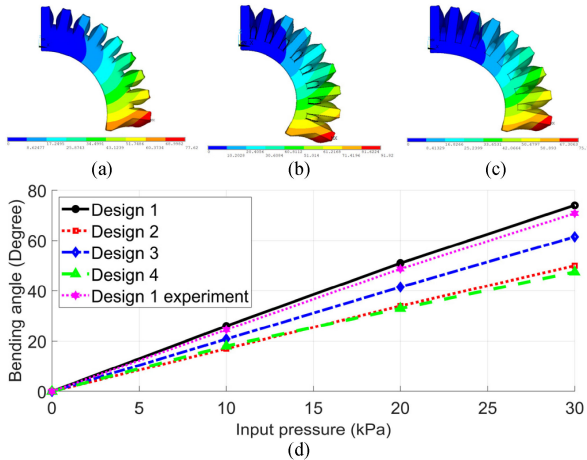

Fig. 8. Results of the analysis. (a) Design 2 deformation contour at 30 kPa. (b) Design 3 deformation contour at 30 kPa. (c) Design 4 deformation contour at 30 kPa. (d) Bending angle versus input pressure curves.

Fig. 10. Bending deformation of the developed soft pneumatic actuator and the commercial SRT actuator at different air pressures. Both actuators have the same length and width.

contours for designs 2, 3, and 4, respectively, at 30 kPa, and Fig. 8(d) shows the bending angle versus the pressure curves of the four designs. It can be observed that the optimized design (Design 1) generates greater deflection (as can be seen in Fig. 6(c)) than designs 2, 3, and 4, which demonstrates the effectiveness of the topology-optimized actuator design in terms of maximizing the bending capability of the soft pneumatic actuator. The bending angle for Design 1 is 50%, 23%, and 52% larger than that for Designs 2, 3 and 4, respectively, on average. In addition, the experimental results for Design 1 are also provided in Fig. 8(d), which show very good agreement with the numerical results, where the average difference between the simulation and experiment is 3%. A detailed description of the prototype and experimental results is provided in the next section.

V. PROTOTYPE AND EXPERIMENTAL RESULTS

The prototype of the optimized soft bending actuator is shown in Fig. 9, which provides the bending deformation of the developed soft actuator under different air pressures (from
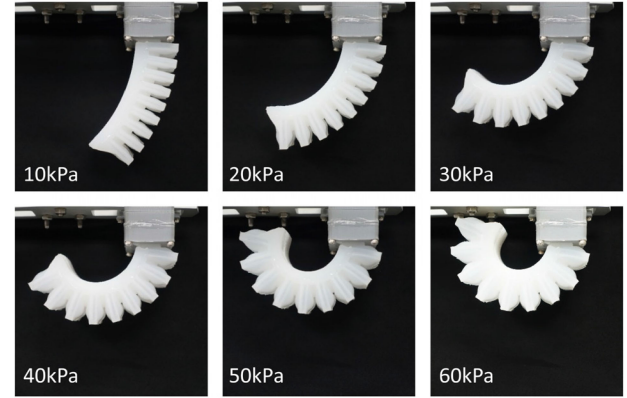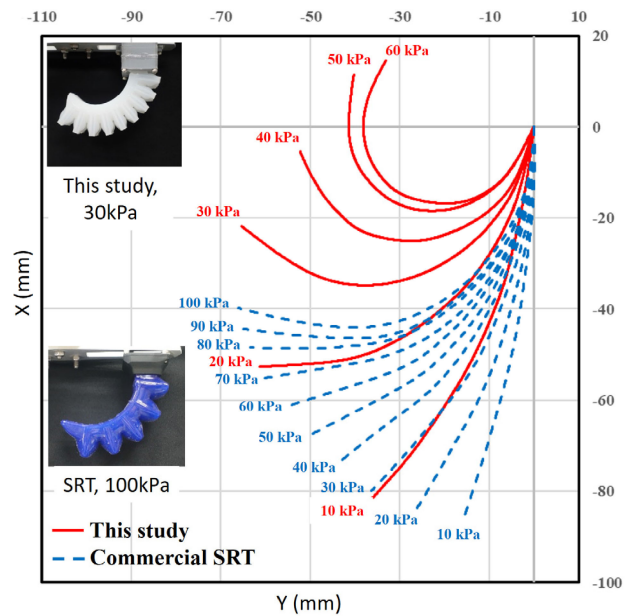
10 kPa to 60 kPa at 10 kPa increments). It can be observed that the embedded chambers inflate to generate the bending motion when the soft actuator is pressurized by the supply air. The bending actuator almost touches the upper fixture when the input pressure is 50 kPa, while contact occurs at a pressure of 60 kPa. In order to compare the capability of the proposed bending actuator with a commercial SRT soft pneumatic bending actuator [37], a series of tests, including bending deformation, output force, and maximum payload, are carried out. Fig. 10 shows a comparison of the bending deformation for the developed soft pneumatic actuator and the commercial SRT actuator at different air pressures, where the bending conditions are measured from the contact surfaces of both actuators and obtained through image processing. The selected SRT actuator (SFG-M5086) [37] is shown in Fig. 10. Its width, length, and height are 50 mm, 86 mm, and 26 mm, respectively. From Fig. 10, it can be observed that the soft pneumatic actuator developed in this
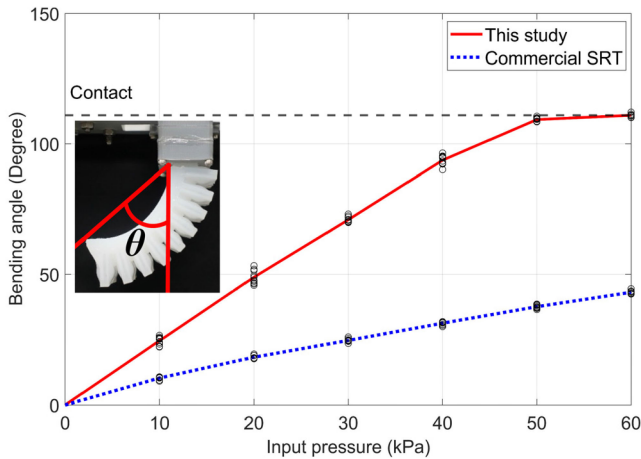
Fig. 11. Bending angle versus input pressure curves: comparison of the experimental results for the developed soft pneumatic actuator and the commercial SRT actuator at different air pressures (the tests are repeated 10 times at each pressure for each actuator, and the average values are used to draw the trend curves).
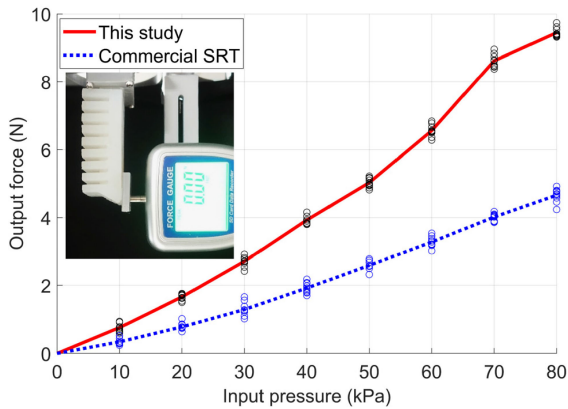

Fig. 12. Output force versus input pressure curves: comparison of the experimental results for the developed soft pneumatic actuator and the commercial SRT actuator at different air pressures (the tests are repeated 10 times at each pressure for each actuator, and the average values are used to draw the trend curves).

study can generate a greater amount of bending deformation at a lower input pressure as compared to the commercial SRT actuator. The bending deformation of the developed actuator at an input pressure of 30 kPa exceeds the bending deformation of the commercial SRT actuator at an input pressure of 100 kPa.

Fig. 11 shows a comparison of the bending angles from the developed actuator and the commercial SRT actuator at different air pressures. The tests are repeated 10 times at each pressure, and the average values are used to draw the trend curves. The average variations of the bending angles for the developed and the commercial bending actuators are 2.6% and 2.2%, respectively, comparing to the average values. It can be observed that the bending angle, denoted as θ in Fig. 11 for the developed actuator, is 177% larger than that for the commercial SRT actuator, on average, at input pressures ranging from 10 kPa to 50 kPa. The average bending angle for the commercial SRT actuator is 37.6° at a pressure of 50 kPa, whereas the bending angle for the developed bending actuator is 109.3° at the same
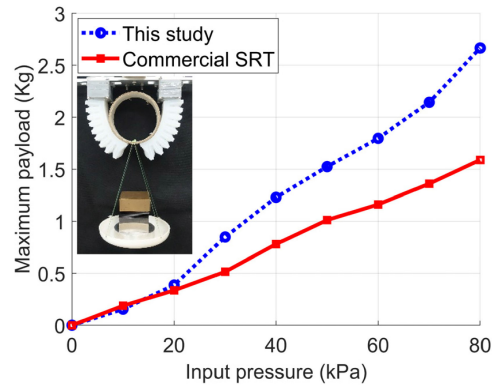

Fig. 13. Maximum payload for a two-fingered gripper with two identical soft pneumatic bending actuators: comparison of the experimental results for the developed soft pneumatic actuator and the commercial SRT actuator at different air pressures.

supply pressure, which is 191% greater than that for the SRT actuator.

To evaluate the output force of the bending actuator, a Lutron FG-6020SD force gauge was placed (and fixed) at the fingertip to measure the output force at different air pressures. The experimental setup and the measured results are provided in Fig. 12. The tests are repeated 10 times at each pressure for each actuator, and the average values are used to draw the trend curves. The average variations of the blocked forces for the developed and the commercial bending actuators are 3.9% and 7.3%, respectively, comparing to the average values. Fig. 12 shows that the output force of the developed actuator is 9.45 N at an input pressure of 80 kPa, while the output force of the commercial SRT actuator is measured as 4.66 N with the same experimental setup. The average output force of the developed bending actuator is 108% higher on average than that of the SRT actuator at input pressures ranging from 10 kPa to 80 kPa at 10 kPa increments.

The developed soft pneumatic bending actuator can be used in robotic grasping applications. To investigate the maximum payload of the two-fingered gripper with two identical soft pneumatic bending actuators, a payload test, as shown in Fig. 13, is carried out to estimate the maximum payload of the two-fingered gripper at different air pressures. The payload tests were performed iteratively by gradually increasing the number of mass blocks in a tray hanging on the gripped object. The maximum payload of the two-fingered gripper with the two developed soft pneumatic bending actuators was found to be 2.66 kg at an input pressure of 80 kPa, whereas the maximum payload of the gripper with two commercial SRT actuators was measured as 1.59 kg. The maximum payload of the developed two-fingered gripper was thus 44% higher on average than the two-fingered SRT gripper at input pressures ranging from 10 kPa to 80 kPa at 10 kPa increments.

Fig. 14 shows the payload test results for the three-fingered grippers. The maximum payload of the three-fingered gripper with three developed soft pneumatic bending actuators was identified as 5.12 kg at an input pressure of 80 kPa, whereas the maximum payload of the gripper with three commercial SRT actuators was measured as 2.22 kg. The maximum payload of the developed three-fingered gripper was 140% higher on average than the three-fingered SRT gripper at input pressures ranging from 10 kPa to 80 kPa at 10 kPa increments.
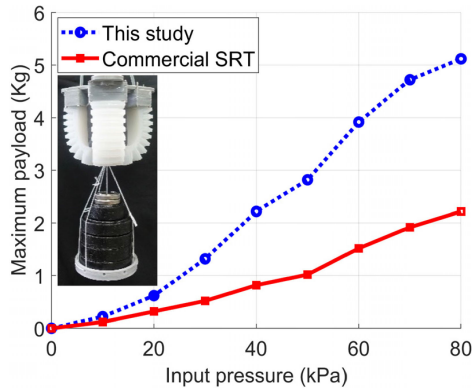
Fig. 14. Maximum payload for a three-fingered gripper with three identical soft pneumatic bending actuators: comparison of the experimental results for the developed soft pneumatic actuator and the commercial SRT actuator at different air pressures.
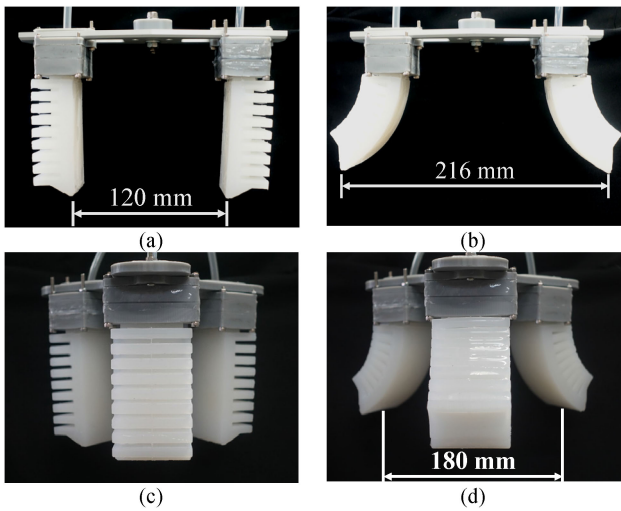

Fig. 15. Two-fingered and three-fingered soft pneumatic grippers. (a) Initial conditions for the two-fingered gripper with two identical soft pneumatic bending actuators. (b) Open mode of the two-fingered gripper. (c) Initial conditions for the three-fingered gripper with three identical soft pneumatic bending actuators. (d) Open mode of the three-fingered gripper.

Fig. 15(a) and (b) show the initial condition and open mode, respectively, for the two-fingered gripper. Fig. 15(c) and (d) show the initial condition and open mode for the three-fingered gripper, respectively. The open modes for the two-fingered and three-fingered grippers, as shown in Fig. 15(b) and (d), are both at a negative pressure of 200 kPa. Fig. 16 shows the grasping test results for a variety of different objects using the developed two-fingered and three-fingered soft pneumatic grippers.

The objects used in the two-fingered grasping test included a toy, a light bulb, a head of broccoli, noodles wrapped in cellophane, a canned soft drink, and a mandarin orange, whereas the objects used in the three-fingered grasping test include a mandarin orange, a head of broccoli, a toy, paper towels, a bottle of sauce, and a package of tissues. The experimental results demonstrated that the two-fingered and three-fingered soft pneumatic grippers developed in this research can be used for handling these irregular or delicate objects.
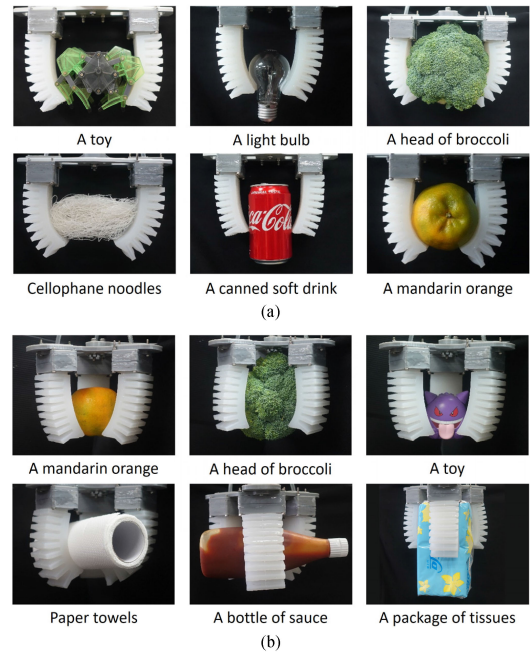

Fig. 16. Grasping test results for a variety of different objects. (a) Two-fingered gripper. (b) Three-fingered gripper.

VI. CONCLUSION

This study presents a design for a soft pneumatic bending actuator using a 3D topology optimization procedure. One segment of the soft pneumatic bending actuator with three air chambers is used as the analysis domain for the topology optimization. The developed bending actuator consisted of three optimized finger segments in series, a fingertip structure, and a contact surface structure. To investigate the effectiveness of the topology-optimized design, three additional actuator designs with different interface structures were analyzed via a geometrically nonlinear finite element analysis in order to compare their maximum bending angles at different input pressures. The numerical results showed that the bending angle for the optimized design is 50%, 23%, and 52% greater than that for the other three designs, respectively, on average. In addition, the average difference in the bending angle between the simulation and the experiment for the optimized actuator design was 3%.

Both two-fingered and three-fingered soft grippers were developed using the topology-optimized bending actuators. The experimental results showed that the soft pneumatic bending actuator developed in this work is superior to the commercial SRT actuator in terms of maximizing the bending angle and the output force. In addition, the developed soft pneumatic actuator can be operated at a lower supply pressure ranging from 10 kPa to 50 kPa while correspondingly generating a bending angle ranging from 25° to 111° on average of 10 tests. The bending angle for the developed actuator was 177% greater than that for the commercial SRT actuator on average at input pressures ranging from 10 kPa to 50 kPa. The output force of the developed actuator reached 9.45 N on average of 10 tests at an input pressure of 80 kPa, while the output force of the commercial SRT actuator was measured as 4.66 N under the same experimental setup conditions. The output force for the developed actuator was 108% greater than that for the commercial SRT actuator on average at input pressures ranging from 10 kPa to 80 kPa.

The maximum payload of the developed two-fingered soft pneumatic gripper was 44% higher on average than the two-fingered SRT gripper at input pressures ranging from 10 kPa to 80 kPa at 10 kPa increments, whereas the maximum payload of the developed three-fingered gripper was 140% higher on average than the three-fingered SRT gripper. The maximum load capacities of the two-fingered and three-fingered grippers were found to be 2.66 kg and 5.12 kg, respectively, at an input pressure of 80 kPa.

The presented optimization method is limited to static and linear problems without considering the effects of geometric and material nonlinearities, as well as the dynamic behavior under different supply pressures. Although the proposed optimal design is synthesized under the assumption of small deformation and linear elasticity, we use geometrically nonlinear FEA and experiments to prove that the design still has better performance under large deformation conditions. In addition to resolving the above limitations, possible future research may include, for example, considering the connecting channel for the air chambers during optimization, and using a whole actuator as a design domain to identify the optimal design.

REFERENCES

[1] J. Shintake, V. Cacucciolo, D. Floreano, and H. Shea, "Soft robotic grippers," *Adv. Mater.*, vol. 30, no. 29, 2018, Art. no. 1707035.

[2] T. Hainsworth, L. Smith, S. Alexander, and R. MacCurdy, "A fabrication free, 3d printed, multi-material, self-sensing soft actuator," *IEEE Robot. Automat. Lett.*, vol. 5, no. 3, pp. 4118–4125, Jul. 2020.

[3] H. K. Yap, H. Y. Ng, and C. H. Yeow, "High-force soft printable pneumatics for soft robotic applications," *Soft Robot.*, vol. 3, no. 3, pp. 144–158, 2016.

[4] F. Chen *et al.*, "Topology optimized design, fabrication, and characterization of a soft cable-driven gripper," *IEEE Robot. Automat. Lett.*, vol. 3, no. 3, pp. 2463–2470, Jul. 2018.

[5] C. -H. Liu *et al.*, "Optimal design of a soft robotic gripper for grasping unknown objects," *Soft Robot.*, vol. 5, no. 4, pp. 452–465, 2018.

[6] H. Zhang, A. S. Kumar, J. Y. H. Fuh, and M. Y. Wang, "Design and development of a topology-optimized three-dimensional printed soft gripper," *Soft Robot.*, vol. 5, no. 5, pp. 650–661, 2018.

[7] C. -H. Liu, F. -M. Chung, Y. Chen, C. -H. Chiu, and T. -L. Chen, "Optimal design of a motor-driven three-finger soft robotic gripper," *IEEE/ASME Trans. Mechatronics*, vol. 25, no. 4, pp. 1830–1840, Aug. 2020.

[8] H. Zhu *et al.*, "Weight imprinting classification-based force grasping with a variable-stiffness robotic gripper," *IEEE Trans. Automat. Sci. Eng.*, to be published, doi: 10.1109/TASE.2021.3054655.

[9] M. Honarpardaz, M. Tarkian, J. Ölvander, and X. Feng, "Finger design automation for industrial robot grippers: A review," *Robot. Auton. Syst.*, vol. 87, pp. 104–119, 2017.

[10] J. Bohg, A. Morales, T. Asfour, and D. Kragic, "Data-Driven grasp Synthesis-A survey," *IEEE Trans. Robot.*, vol. 30, no. 2, pp. 289–309, Apr. 2014.

[11] D. Trivedi, C. D. Rahn, W. M. Kier, and I. D. Walker, "Soft robotics: Biological inspiration, state of the art, and future research," *Appl. bionics Biomech.*, vol. 5, no. 3, pp. 99–117, 2008.

[12] S. Kim, C. Laschi, and B. Trimmer, "Soft robotics: A bioinspired evolution in robotics," *Trends Biotechnol.*, vol. 31, pp. 287–294, 2013.

[13] J. Ma *et al.*, "Integrated mechatronic design in the flexure-linked dual-drive gantry by constrained linear–quadratic optimization," *IEEE Trans. Ind. Electron.*, vol. 65, no. 3, pp. 2408–2418, Mar. 2018.

[14] S. L. Chen, X. Li, C. S. Teo, and K. K. Tan, "Composite jerk feedforward and disturbance observer for robust tracking of flexible systems," *Automatica*, vol. 80, pp. 253–260, 2017.

[15] C. du Pasquier, T. Chen, S. Tibbits, and K. Shea, "Design and computational modeling of a 3D printed pneumatic toolkit for soft robotics," *Soft Robot.*, vol. 6, no. 5, pp. 657–663, 2019.

[16] Z. Wang, Y. Torigoe, and S. Hirai, "A prestressed soft gripper: Design, modeling, fabrication, and tests for food handling," *IEEE Robot. Automat. Lett.*, vol. 2, no. 4, pp. 1909–1916, Oct. 2017.

[17] Z. Wang, K. Or, and S. Hirai, "A dual-mode soft gripper for food packaging," *Robot. Auton. Syst.*, vol. 125, 2020, Art. no. 103427.

[18] K. -M. Lee, "Design criteria for developing an automated live-bird transfer system," *IEEE Trans. Robot. Automat.*, vol. 17, no. 4, pp. 483–490, Aug. 2001.

[19] C. -H. Liu and K. -M. Lee, "Dynamic modeling of damping effects in highly damped compliant fingers for applications involving contacts," *ASME J. Dynamic Syst., Meas. Control*, vol. 134, 2012, Art. no. 011005.

[20] K. -M. Lee and C. -H. Liu, "Explicit dynamic finite element analysis of an automated grasping process using highly damped compliant fingers," *Comput. Math. Appl.*, vol. 64, pp. 965–977, 2012.

[21] Y. Liu, Y. Zhang, and Q. Xu, "Design and control of a novel compliant constant-force gripper based on buckled fixed-guided beams," *IEEE/ASME Trans. Mechatronics*, vol. 22, no. 1, pp. 476–486, Feb. 2017.

[22] C. -H. Liu, M. -C. Hsu, T. -L. Chen, and Y. Chen, "Optimal design of a compliant constant-force mechanism to deliver a nearly constant output force over a range of input displacements," *Soft Robot.*, vol. 7 , no. 6, pp. 758–769, 2020.

[23] C. -H. Liu, F. -M. Chung, and Y. -P. Ho, "Topology optimization for design of a 3D-printed constant-force compliant finger," *IEEE/ASME Trans. Mechatronics*, vol. 26, no. 4, pp. 1828–1836, Aug. 2021.

[24] K. C. Galloway *et al.*, "Soft robotic grippers for biological sampling on deep reefs," *Soft Robot.*, vol. 3, no. 1, pp. 23–33, 2016.

[25] D. Mura, M. Barbarossa, G. Dinuzzi, G. Grioli, A. Caiti, and M. G. Catalano, "A soft modular end effector for underwater manipulation: A gentle, adaptable grasp for the ocean depths," *IEEE Robot. Automat. Mag.*, vol. 25, no. 4, pp. 45–56, Dec. 2018.

[26] H. Zhang, A. S. Kumar, F. Chen, J. Y. Fuh, and M. Y. Wang, "Topology optimized multimaterial soft fingers for applications on grippers, rehabilitation, and artificial hands," *IEEE/ASME Trans. Mechatronics*, vol. 24, no. 1, pp. 120–131, Feb. 2019.

[27] C. -H. Liu, C. -H. Chiu, T. -L. Chen, T. -Y. Pai, M. -C. Hsu, and Y. Chen, "Topology optimization and prototype of a three-dimensional printed compliant finger for grasping vulnerable objects with size and shape variations," *ASME J. Mechanisms Robot.*, vol. 10, 2018, Art. no. 044502.

[28] C. -H. Liu, G. -F. Huang, C. -H. Chiu, and T. -Y. Pai, "Topology synthesis and optimal design of an adaptive compliant gripper to maximize output displacement," *J. Intell. Robotic Syst.*, vol. 90, no. 3/4, pp. 287–304, 2018.

[29] C. -H. Liu, C. -H. Chiu, M. -C. Hsu, Y. Chen, and Y. -P Chiang, "Topology and size–shape optimization of an adaptive compliant gripper with high mechanical advantage for grasping irregular objects," *Robotica*, vol. 37, no. 8, pp. 1383–1400, 2019.

[30] C. -H. Liu, T. -L. Chen, T. -Y. Pai, C. -H. Chiu, W. -G. Peng and C. -C. Weng , "An intelligent robotic system for handling and laser marking fruits," in *Technologies and Eco-Innovation Towards Sustainabilityin I*, Singapore: Springer, 2019, pp. 75–88.

[31] L. Marechal, P. Balland, L. Lindenroth, F. Petrou, C. Kontovounisios, and F. Bello, "Toward a common framework and database of materials for soft robotics," *Soft Robot.*, vol. 8, no. 3, pp. 284–297, 2021.

[32] Z. Xie *et al.*, "Octopus arm-inspired tapered soft actuators with suckers for improved grasping," *Soft Robot.*, vol. 7, no. 5, pp. 639–648, 2020.

[33] C. B. W. Pedersen, N. A. Fleck, and G. K. Ananthasuresh, "Design of a compliant mechanism to modify an actuator characteristic to deliver a constant output force," *ASME J. Mech. Des.*, vol. 128, pp. 1101–1112, 2006.

[34] A. T. Gaynor, N. A. Meisel, C. B. Williams, and J. K. Guest, "Multiple-material topology optimization of compliant mechanisms created via polyjet three-dimensional printing," *ASME J. Manuf. Sci. Eng.*, vol. 136, no. 6, 2014, Art. no. 061015.

[35] C. -H. Liu and G. -F. Huang, "A topology optimization method with constant volume fraction during iterations for design of compliant mechanisms," *ASME J. Mechanisms Robot.*, vol. 8, no. 4, 2016, Art. no. 044505.

[36] C. -H. Liu, G. -F. Huang, and T. -L. Chen, "An evolutionary soft-add topology optimization method for synthesis of compliant mechanisms with maximum output displacement," *ASME J. Mechanisms Robot.*, vol. 9, no. 5, 2017, Art. no. 054502.

[37] [Online]. Available: https://www.softrobottech.com/

[38] O. Sigmund, "Morphology-based black and white filters for topology optimization," *Struct. Multidisciplinary Optim.*, vol. 33, no. 4/5, pp. 401–424, 2007.

[39] K. Svanberg, "The method of moving asymptotes—A new method for structural optimization," *Int. J. Numer. Methods Eng.*, vol. 24, no. 2, pp. 359–373, 1987.